Chinese Chemical Letters 35 (2024) 108881

Contents lists available at ScienceDirect

Chinese Chemical Letters

journal homepage: www.elsevier.com/locate/cclet

Discovery of unusual phloroglucinol–triterpenoid adducts from *Leptospermum scoparium* and *Xanthostemon chrysanthus* by building blocks-based molecular networking

Jinyan Zhang[a,b,1], Fen Liu[a,b,1], Qian Jin[c], Xueyi Li[a,b], Qiong Zhan[a,b], Mu Chen[a,b], Sisi Wang[a,b], Zhenlong Wu[a,b,*], Wencai Ye[a,b,*], Lei Wang[a,b,*]

[a] State Key Laboratory of Bioactive Molecules and Druggability Assessment, Jinan University, Guangzhou 510632, China
[b] Center for Bioactive Natural Molecules and Innovative Drugs, and Guangdong Province Key Laboratory of Pharmacodynamic Constituents of TCM and New Drugs Research, Jinan University, Guangzhou 510632, China
[c] College of Pharmacy, Jinan University, Guangzhou 510632, China

ARTICLE INFO

Article history:
Received 24 May 2023
Revised 29 July 2023
Accepted 2 August 2023
Available online 3 August 2023

Keywords:
Phloroglucinol-triterpenoid adduct
Myrtaceae
Building blocks-based molecular network
Biomimetic synthesis
Antiviral activity
Anti-inflammatory activity

ABSTRACT

The first phloroglucinol-triterpenoid hybrids, myrtphlotritins A–E (**1**–**5**), were rapidly recognized and isolated from two species of Myrtaceae by employing the building blocks-based molecular network (BBMN) strategy. Compounds **1**–**5** featured new carbon skeletons in which phloroglucinol derivatives were coupled with lupane- and dammarane-type triterpenoids through different linkage patterns. Their structures and absolute configurations were elucidated by comprehensive analysis of spectroscopic data and quantum chemical calculations. Biosynthetic pathways for compounds **1**–**5** were proposed on the basis of the coexisting precursors. Guided by the biogenetic pathways, the biomimetic synthesis of compound **1** was also achieved. Additionally, compounds **2**, **3**, and **5** exhibited potent antiviral activities against herpes simplex virus type-1 (HSV-1) infection, and compounds **2** and **5** displayed significant anti-inflammatory activities on RAW264.7 cells.

Phloroglucinol derivatives are typical secondary metabolites accumulated in the families Myrtaceae, Guttiferae, and Euphorbiaceae, which have shown broad bioactivities such as antimicrobial, anti-inflammatory, and antitumor effects [1–6]. Hitherto, over 2000 members of phloroglucinol derivatives have been reported [1–3]. Among them, the phloroglucinol–terpenoid adducts (PTAs) had drawn extensive considerations from both the chemical and biological communities, due to their diverse carbon skeletons and remarkable biological effects [4–7]. Biosynthetically, PTAs are commonly hypothesized to form by the coupling of the *ortho*-quinone methide (*o*-QM) and terpenoid intermediates [4–7]. For the latter, it is well known that monoterpenoid [8], sesquiterpenoid [9,10], and diterpenoid moieties [11] can incorporate with *o*-QM to form the PTA architectures through different combinational patterns. However, as one of the largest and widely occurred motifs in plant secondary metabolites, the triterpenoid fragments have never been described in PTAs, leaving them as the missing pieces of the diversified PTAs family so far.

During the course of our continuing study on phloroglucinol derivatives from plants of family Myrtaceae, a number of novel PTAs with distinguished structural features and significant bioactivities were isolated, some of which had also been biomimetically synthesized [7-9,12-15]. Recently, in order to discover natural products more efficiently, the building blocks-based molecular network (BBMN) strategy was presented by our group [16]. This strategy is based on the principle that natural products are comprised by specific precursors and display correspondent characteristic fragments in their tandem mass spectra. To further explore the unknown chemical space of PTAs, a BBMN-guided phytochemical investigation on two species of Myrtaceae plants, *Leptospermum scoparium* and *Xanthostemon chrysanthus*, was carried out. As a result, five unprecedented phloroglucinol-triterpenoid adducts, myrtphlotritins A–E (**1**–**5**), were identified (Fig. 1). To the best of our knowledge, these isolates represented the first examples of phloroglucinol-triterpenoid adducts in the PTAs kingdom. Specifically, compounds **1**–**3** from *L. scoparium* incorporated a phenylpropanoyl-triketone motif with a lupane-type pentacyclic triterpenoid unit *via* two different linkage patterns. Compounds **4**

* Corresponding authors.
E-mail addresses: zhenlongwu@jnu.edu.cn (Z. Wu), chywc@aliyun.com (W. Ye), cpuwanglei@126.com (L. Wang).
[1] These authors contributed equally to this work.

https://doi.org/10.1016/j.cclet.2023.108881
1001-8417/

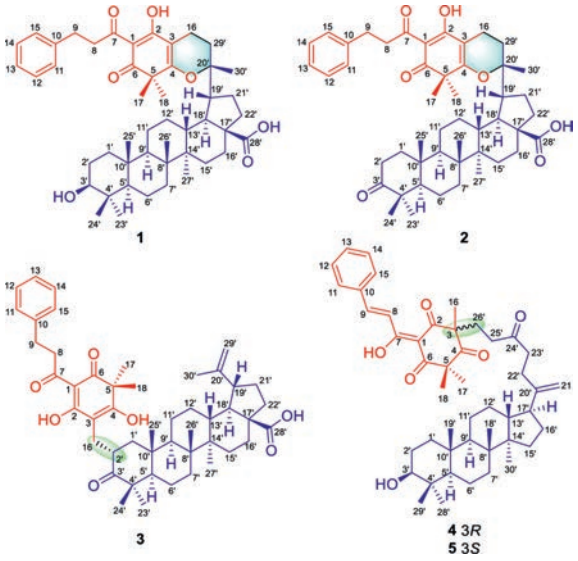

Fig. 1. Chemical structures of myrtphlotritins A–E (**1**–**5**).

and **5** from *X. chrysanthus* constituted a pair of epimers, in which a phenylpropanoyl-triketone moiety and a dammarane-type tetracyclic nortriterpenoid unit were bridged through a carbon-carbon bond. Herein, we reported the discovery, structure elucidation, and hypothetical biogenetic pathways of these novel phloroglucinol-triterpenoid adducts. Additionally, the biomimetic synthesis of compound **1**, as well as the antiviral and anti-inflammatory activities of **1**–**5** were discussed.

The liquid chromatography-tandem mass spectrometry (LC-MS^2) data of the petroleum ether fractions of the flowers of *L. scoparium* and the leaves of *X. chrysanthus* were respectively acquired on an ultra high performance liquid chromatography (UHPLC) tandem Orbitrap instrument. Initially, the featured-based molecular networking (FBMN) was employed to annotate the known compounds from the acquired LC-MS^2 data [17]. As a result, several phloroglucinols together with terpenes were rapidly identified from the above two fractions, indicating the existence of two biogenetic precursors of PTAs in the plants. To obtain the diagnostic ions for BBMN, the electrospray ionization tandem mass spectra of PTAs in our compound library were analysed, which afforded the characteristic product ions at *m/z* 195.065 (Fig. S1 in Supporting information) and 95.086 (corresponding to the phenylpropanoyl-triketone motif and terpene unit, respectively) [18]. Despite the characteristic ions for triterpenoids were not identified, the larger molecular weights of triterpenoids than mono- and diterpenoids might be a suitable indication. Hence, two diagnostic ions at *m/z* 195.065 and 95.086 were used to filtrate the LC-MS^2 data of the extracts, and their BBMN networks were constructed, respectively. As depicted in Fig. 2, the networks showed several nodes with distinguished MS^2 features and larger molecular weights (red ones), which were selected as targets for further investigation. Following a LC-MS guided isolation procedure, we finally obtained the target compounds **1**–**5**.

Myrtphlotritin A (**1**) was isolated as an amorphous powder. The molecular formula of **1** was determined as $C_{48}H_{66}O_7$ by its high-resolution electrospray ionization mass spectrometry (HR-ESI-MS) data at *m/z* 755.4879 $[M+H]^+$ (calcd. for $C_{48}H_{67}O_7$, 755.4881), corresponding to 16 degrees of unsaturation. The ultraviolet (UV) spectrum displayed the absorption maxima at 205 and 337 nm. The infrared (IR) spectrum showed the typical absorptions of carbonyl (1736 cm^{-1}) and benzene ring (1653 and 1456 cm^{-1}). The ^1H and ^{13}C nuclear magnetic resonance (NMR) spectra of **1** revealed the existence of two carbonyls, a monosubstituted benzene ring group,

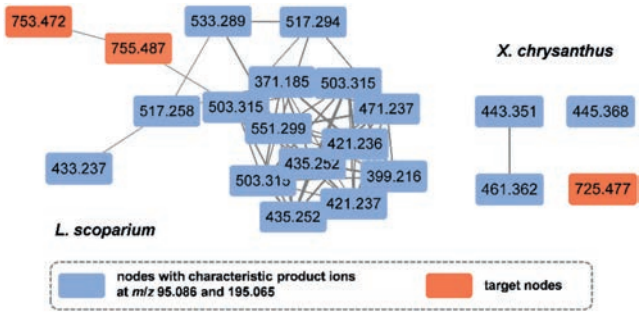

Fig. 2. The building blocks-based networks for the petroleum ether fractions of the flowers of *L. scoparium* and the leaves of *X. chrysanthus*.

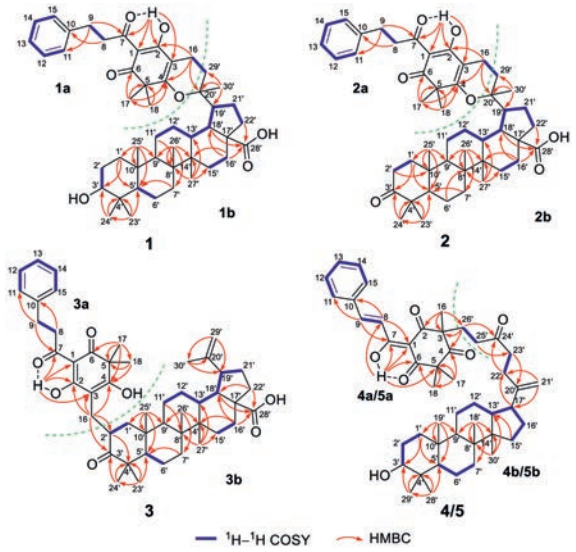

Fig. 3. ^{1}H–^{1}H COSY and key HMBC correlations of **1**–**5**.

and eight methyl groups. Analyses of one- and two-dimensional (1D and 2D) NMR data resulted in the full assignments of the ^1H and ^{13}C NMR signals of **1** (Table S1 in Supporting information).

Interpretation of the ^1H–^1H correlation spectroscopy (^1H–^1H COSY) spectrum of **1** revealed the presence of seven spin-coupling systems (Fig. 3). In the heteronuclear multiple bond correlation (HMBC) spectrum, the key correlations between 2-OH and C-1/C-2/C-3/C-7, between H_2–8 and C-10, between H_2–9 and C-7/C-11, between H_2–16 and C-2/C-4, between H_3–17 and C-4/C-5/C-6, as well as between H_3–18 and C-4/C-5/C-17 indicated the presence of a phenylpropanoyl-β-triketone unit (**1a**) in **1** [19]. Additionally, the key HMBC cross peaks between H_2–1′ and C-3′/C-5′, between H_3–24′ and C-3′/C-4′, between H_3–23′ and C-4′/C-5′/C-24′, between H_3–25′ and C-1′/C-5′/C-9′/C-10′, between H_2–7′ and C-5′, between H_2–11′ and C-8′, between H_3–26′ and C-7′/C-8′/C-9′/C-14′, between H_3–27′ and C-8′/C-13′/C-14′/C-15′, between H_2–16′ and C-14′/C-18′, between H_2–16′/H-18′/H_2–22′ and C-28′, as well as between H_3–30′ and C-19′/C-20′/C-29′, suggested the presence of a lupane-type pentacyclic triterpenoid unit (**1b**) [20]. Moreover, the key HMBC correlation between H_2–16 and C-20′ revealed the C-16—C-29′ linkage between **1a** and **1b**. The above assignments accounted for 15 out of the 16 degrees of unsaturation in **1**. The remaining one degree of unsaturation, together with the obvious downfield shift of the sp^3-hybridized quaternary carbon C-20′ (δ_C 83.7) and molecular weight information, suggested that C-4 and

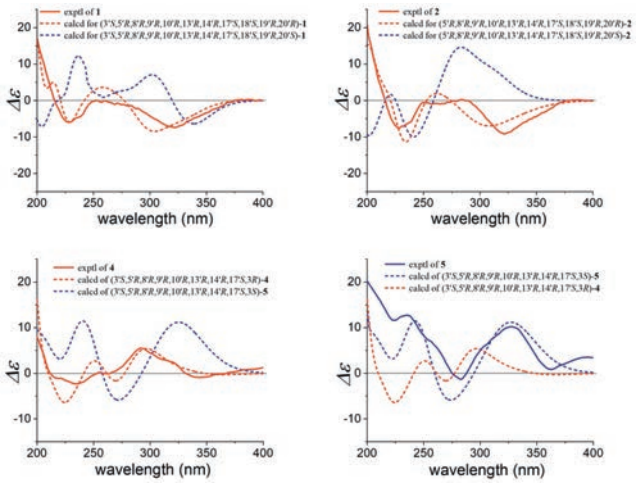

Fig. 4. Experimental and calculated ECD spectra of **1**, **2**, **4**, and **5**.

C-20′ were connected *via* an oxygen atom to form a pyran ring. Hence, the planar structure of **1** was established.

In the nuclear overhauser effect spectroscopy (NOESY) experiment of **1**, the key nuclear overhauser effect (NOE) cross peaks (Fig. S2 in Supporting information) showed a similar pattern to those observed in the known compound betulinic acid [20], which allowed the determination of the configurations of all stereocenters except for C-20′. To solve it, the theoretical ^{13}C NMR chemical shifts of the two possible stereoisomers 20′*R*-**1** and 20′*S*-**1** were calculated using the GIAO method [21] at the mPW1PW91/6–311+G(d,p) level, respectively. The calculated ^{13}C NMR chemical shifts for two C-20′ epimers of **1** were corrected using the provided slope and intercept values, and the difference between the corrected and experimental data were further evaluated. With a DP4+ probability of 100% for the 20′*R* configuration, the configuration of C-20′ was determined as *R* (Fig. S2). Finally, the absolute configuration of **1** was confirmed by comparison of the theoretical electronic circular dichroism (ECD) curves with the experimental one (Fig. 4).

The molecular formula of myrtphlotritin B (**2**) was deduced to be $C_{48}H_{64}O_7$ by its HR-ESI-MS data at *m/z* 753.4732 $[M+H]^+$ (calcd. for $C_{48}H_{65}O_7$, 753.4725). Comparison of the ^{1}H and ^{13}C NMR data of **2** (Table S1) with those of **1** revealed their similarity, except that the hydroxylated carbon (δ_C 79.1, δ_H 3.19) in the triterpenoid section of **1** were replaced by a carbonyl carbon (δ_C 218.1) in **2**, suggesting that **2** was a 3′-one derivative of **1** [20]. The above assignments were further ascertained by extensive 2D NMR experiments including the ^{1}H–^{1}H COSY, HMBC, and NOESY (Fig. 3 and Fig. S3 in Supporting information). Using a similar gauge-including atomic orbital (GIAO) method described for **1**, the calculated ^{13}C NMR data allowed the determination of C-20′ configuration as *R*, based on a DP4+ probability of 100% (Fig. S2). Furthermore, the absolute configuration of **2** was ascertained to be 5′*R*,8′*R*,9′*R*,10′*R*,13′*R*,14′*R*,17′*S*,18′*S*,19′*R*,20′*R* according to the matched ECD curves between the calculated and experimental ones (Fig. 4).

The molecular formula of myrtphlotritin C (**3**) was also assigned as $C_{48}H_{64}O_7$ by its HR-ESI-MS data at *m/z* 753.4729 $[M+H]^+$ (calcd. for $C_{48}H_{65}O_7$, 753.4725), suggested that **3** is an isomer of **2**. Comparison of the 1D and 2D NMR data of **3** with those of **2** indicated the presence of two moieties (**3a** and **3b**) in **3** deriving from phenylpropanoyl-β-triketone and betulonic acid [20], respectively. Differently, the key HMBC correlations between H_2–16 and C-2/C-3/C-4/C-2′/C-3′, revealed that motifs **3a** and **3b** were connected *via* C-2′–C-16 (Fig. 3). In the ROESY spectrum of **3**, the correlations between H_3–25′ and H_3–24′/H_3–26′, between H-5′ and H_3–23′/H-9′, between H_3–27′ and H-9′/H-18′, and between H-13′ and H_3–19′/H-26′ were observed, suggesting that **3** has the same configurations as betulonic acid. In addition, the ROE correlation between H-2′ and H_3–25′ indicated that they were co-facial, which determined the configuration of C-2′ (Fig. S3). The absolute configuration of **3** was further confirmed by ECD calculation (Fig. S4 in Supporting information).

The molecular formula of myrtphlotritin D (**4**) was established as $C_{47}H_{64}O_6$ by its HR-ESI-MS data at *m/z* 725.4785 $[M+H]^+$ (calcd. for $C_{47}H_{65}O_6$, 725.4776). Comprehensive analyses of the 1D and 2D NMR spectroscopic data of **4** led to the full assignments of its proton and carbon resonances (Table S2 in Supporting information). Subsequently, a comparison of the 1D and 2D NMR spectroscopic data of **4** with champanone B [22] and dammara-20,25–dien-3β,24-diol [23] suggested the presence of two units (**4a** and **4b**) deriving from phenylpropanoyl-β-triketone and dammarane-type 27′-nor-triterpenoid, respectively. Besides, the key HMBC correlations between H_2–26′ and C-3/C-4, as well as between H_3–16 and C-26′, indicated that **4a** and **4b** were linked *via* the C-3—C-26′ bond (Fig. 3). The key NOE correlations (Fig. S3) of **4** showed a similar pattern to those observed in dammara-20,25–dien-3β,24-diol [23], indicated the stereochemistry as shown in Fig. 1. To determine the absolute configuration of C-3, the theoretical ECD spectra of two possible stereoisomers of **4** (3*R*-**4** and 3*S*-**4**) were simulated. As a result, the measured ECD spectrum of **4** was in good agreement with the calculated curve of 3*R*-**4**. Thus, the absolute configuration of **4** was determined as 3′*S*,5′*R*,8′*R*,9′*R*,10′*R*,13′*R*,14′*R*,17′*S*,3*R* (Fig. 4).

The molecular formula of myrtphlotritin E (**5**) was deduced to be identical to that of **4**. By comprehensive analysis of its 1D and 2D NMR spectral data (Table S2), the planar structure of **5** was assigned to be identical to **4**. The major difference was chemical shift at C-16 ($\Delta\delta_C$ +1.0), suggesting that **5** could be a C-3 epimer of **4**. According to the well matched ECD curve between the calculated and experimental ones, the absolute configuration of **5** was elucidated as 3′*S*,5′*R*,8′*R*,9′*R*,10′*R*,13′*R*,14′*R*,17′*S*,3*S* (Fig. 4).

It should be noted that the ^{1}H and ^{13}C NMR spectra of compounds **1**–**5** showed some small signals close to the major ones, indicating the presence of a mixture of tautomeric isomers. Several studies, including our previous work, had investigated the inseparable keto-enol and *Z*/*E* geometric tautomerism of phloroglucinol derivatives due to the existence of β,β'-tricarbonyl motifs in the structure [19,22,24]. Similar to the previous reports, the keto-enol and *Z*/*E* geometric tautomerism also existed in **1**–**5** (Fig. S5 in Supporting information).

Compounds **1**–**5** represent the first examples of phloroglucinol-triterpenoid adducts with three types of new carbon skeletons. Based on the co-isolation of the precursors myrigalone A (**6**), betulinic acid (**7**), betulonic acid (**8**) and champanone B (**9**) from the title plants (see Supporting information), plausible biosynthetic pathways for **1**–**5** were proposed in Scheme 1. Briefly, oxidation of **6** could give the *o*-QM intermediate **i**, which could undergo hetero-Diels–Alder reactions with **7** and **8** to afford **1** and **2**, respectively. Meanwhile, intermediate **i** could also couple with **8** to give **3** through a Michael addition reaction. In addition, the oxidation and decarboxylation of dammara-20,25–dien-3β,24-diol [23] could yield nortriterpenoid intermediate **ii** [25], which could couple with **9** to generate **4** and **5** through Michael addition reaction.

To further validate the key step of the proposed biosynthetic pathways, a biomimetic synthesis for **1** was carried out (Scheme S1 in Supporting information). Treatment of myrigalone A (**6**) with betulinic acid (**7**), Ag_2O, and TEMPO in Et_2O at −78 °C, and followed by the reflux in PhMe at 110 °C, the major product in 15% yield was successfully obtained. The ^{1}H and ^{13}C NMR data as well as the ECD curve of the synthetic product were identical to those of myrt-

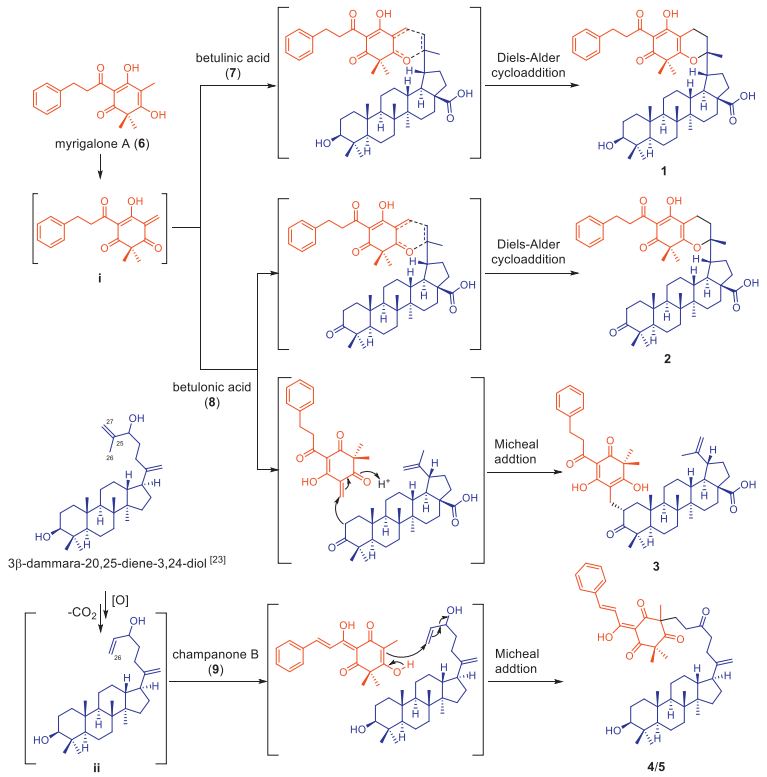

Scheme 1. Plausible biogenetic pathways of **1**–**5**.

phlotritin A (**1**) (Figs. S88–S90 in Supporting information), which further corroborated its chemical structure. Notably, the hetero-Diels-Alder reaction between **6** and **7** exhibited high stereoselectivity, in which the larger triterpenoid group adopted the α conformation rather than the β conformation to yield a major *endo*-type adduct [26].

The isolates were evaluated for their antiviral and anti-inflammatory activities. As shown in Tables S3 (Supporting information), compounds **2**, **3**, and **5** exhibited remarkable anti-herpes simplex virus type-1 (HSV-1) activities with half-maximal inhibitory concentration (IC_{50}) values ranging from 5.96 μmol/L to 19.23 μmol/L with selected indexes (SI) over 5, which were more potent than their precursors (**6**–**9**). Additionally, compounds **2**, **5**, and **8** displayed significant inhibitory effects on the lipopolysaccharide-induced nitric oxide (NO) production in RAW264.7 cells, with IC_{50} values ranging from 9.63 μmol/L to 18.73 μmol/L (Table S4 in Supporting information).

In summary, a BBMN-guided phytochemical investigation on two plants of Myrtaceae had led to the discovery of five phloroglucinol-triterpenoid adducts with unprecedented carbon skeletons. Their structures and absolute configurations were elucidated by comprehensive analysis of spectroscopic data, quantum chemical calculations, and biomimetic synthesis. It is worth noting that these isolates represent the first examples of hybrids of phloroglucinols and triterpenoids in the PTAs family. Besides, the presence of the lupane-type pentacyclic triterpenoid and dammarane-type tetracyclic nortriterpenoid in the molecules revealed the generality of hybridizations between the simple phloroglucinols and various terpenoids, which were not confined to monoterpenoids, sesquiterpenoids, or diterpenoids. Furthermore, compounds **2**, **3** and **5** exhibited potent antiviral activities against HSV-1 infection, while compounds **2** and **5** also showed significant anti-inflammatory activities on RAW264.7 cells. This work furthers our understandings on the structural diversity and biological effects of PTAs.

Declaration of competing interest

The authors declare that they have no known competing financial interests or personal relationships that could have appeared to influence the work reported in this paper.

Acknowledgments

This work was supported by the Guangdong Basic and Applied Basic Research Foundation (Nos. 2020B1515120066 and 2022A1515010010), the National Natural Science Foundation of China [Nos. 82293681 (82293680) and 82273822], the Science and Technology Key Project of Guangdong Province (No. 2020B1111110004), the Local Innovative and Research Teams Project of Guangdong Pearl River Talents Program (No. 2017BT01Y036) and the Fundamental Research Funds for the Central Universities. The author (Zhenlong Wu) also gratefully acknowledges the support of K. C. Wong Education Foundation.

Supplementary materials

Supplementary material associated with this article can be found, in the online version, at doi:10.1016/j.cclet.2023.108881.

References

[1] Y.L. Phang, S. Liu, C.W. Zheng, H.X. Xu, Nat. Prod. Rep. 39 (2022) 1766–1802.
[2] G. Peron, A.M. Lopez, P. Cabada-Aquirre, et al., Crit. Rev. Biotechnol. 44 (2024) 319–336.
[3] F. Khan, N. Tabassum, N.I. Bamunuarachchi, Y.M. Kim, J. Agric. Food Chem. 70 (2022) 4817–4838.
[4] O. Celaj, A.G. Duran, P. Cennamo, et al., Phytochem. Rev. 20 (2021) 259–299.
[5] H. Bridi, G.D. Meirelles, G.L. von Poser, Phytochemistry 155 (2018) 203–232.
[6] I.P. Singh, S.B. Bharate, Nat. Prod. Rep. 23 (2006) 558–591.
[7] J.G. Song, J.C. Su, Q.Y. Song, et al., Org. Lett. 21 (2019) 9579–9583.
[8] J.Q. Cao, H.Y. Tian, M.M. Li, et al., J. Nat. Prod. 81 (2018) 57–62.
[9] J.H. Gu, W.J. Wang, J.Z. Chen, et al., Org. Lett. 22 (2020) 1796–1800.
[10] J. Huang, C. Li, J. Ma, et al., Chin. Chem. Lett. 32 (2021) 1721–1725.

[11] R. Xie, L. Li, X. Fan, J. Zi, Chin. Chem. Lett. 31 (2020) 431–433.
[12] J.Q. Cao, X.J. Huang, Y.T. Li, et al., Org. Lett. 18 (2016) 120–123.
[13] C. Liu, S. Ang, X.J. Huang, et al., Org. Lett. 18 (2016) 4004–4007.
[14] M.J. Cheng, J.Q. Cao, X.Y. Yang, et al., Chem. Sci. 9 (2018) 1488–1495.
[15] M.J. Cheng, X.Y. Yang, J.Q. Cao, et al., Org. Lett. 21 (2019) 1583–1587.
[16] Q.F. He, Z.L. Wu, L.R. Li, et al., Angew. Chem. Int. Ed. 60 (2021) 19609–19613.
[17] L.F. Nothias, D. Petras, R. Schmid, et al., Nat. Methods 17 (2020) 905–908.
[18] J. Uddin, A.B. Muhsinah, M. Imran, M.N. Khan, S.G. Musharraf, Rapid Commun. Mass Spectrom. 36 (2022) e9243.
[19] D.P. Killeen, L. Larsen, F.E. Dayan, et al., J. Nat. Prod. 79 (2016) 564–569.
[20] D.Z.L. Bastos, I.C. Pimentel, D.A. de Jesus, B.H. de Oliveira, Phytochemistry 68 (2007) 834–839.
[21] J. Ma, G. Xia, Y. Zang, et al., Chin. Chem. Lett. 32 (2021) 1173–1176.
[22] Q. Zhan, Y.Y. Wu, F. Liu, et al., Chem. Biodivers. 19 (2022) e202200356.
[23] H.J. Zhang, G.T. Tan, V.D. Hoang, et al., J. Nat. Prod. 66 (2003) 263–268.
[24] K. Xia, J.J. Gu, X.X. Fu, et al., Chem. Biodivers. 19 (2021) e2100252.
[25] S.S. Huang, K.L. Jian, R.J. Li, et al., RSC Adv. 6 (2016) 6320–6328.
[26] I. Fernández, F.M. Bickelhaupt, J. Comput. Chem. 35 (2013) 371–376.